ADVANCED OPTICAL MATERIALS
www.advopticalmat.de

Donor N-Substitution as Design Principle for Fast and Blue Luminescence in Carbene-Metal-Amides

Antti-Pekka M. Reponen, Florian Chotard, Aku Lempelto, Vitalii Shekhovtsev, Dan Credgington, Manfred Bochmann, Mikko Linnolahti, Neil C. Greenham,* and Alexander S. Romanov**

A series of gold-centered carbene-metal-amide (CMA) complexes are synthesized with the carbazole donor ligand modified by substitution with nitrogen atoms in varying positions. The luminescence of new aza-CMA complexes shows a significant blueshift depending on the position of the N atom, to provide bright blue-green (500 nm), sky-blue (478 nm), blue (450 nm) and deep-blue (419 nm) light-emitters. The impact of the electron-withdrawing aza-group on the nature of the luminescence and the excited state energies of the locally excited (LE) or charge transfer (CT) states have been interpreted with the help of transient absorption, in-depth photoluminescence experiments and theoretical calculations. By considering the orbital characters of the lowest CT and LE states, we develop a new concept for simultaneous energy tuning for both of these states with a single aza-substitution, allowing for fast and blue CT emission. This concept allows the interference of ^{3}LE phosphorescence to be avoided at room temperature. The approach is extended to two N substitutions at the optimal location in the 3- and 6-positions of the carbazole skeleton. These results suggest a practical molecular design towards the development of bright and deep-blue emitting CMA materials to tackle the stability problem of energy-efficient deep-blue OLEDs.

1. Introduction

Carbene-metal-amides (CMAs)[1–18] have recently emerged as a new type of donor-bridge-acceptor materials demonstrating unity luminescence quantum yields and short excited state lifetime (<1 µs) and show great promise for realizing energy efficient organic light-emitting diodes (OLEDs). The molecular design of CMA emitters is reminiscent of the donor–acceptor strategy applied in organic thermally activated delayed fluorescence (TADF) materials.[19,20] Organic TADF materials have attracted enormous research interest since Adachi et al. showed they could be used in high-efficiency OLED devices.[20] Unlike organic TADF emitters, the carbene (acceptor) and amide (donor) ligands in CMA materials are bridged by a coinage metal atom that not only enables rotational flexibility between donor and acceptor but also, by virtue of its spin-orbit coupling (SOC) coefficient, greatly accelerates intersystem crossing (ISC) rates, leading to short excited state lifetimes. Since the highest occupied molecular orbital (HOMO) is mainly localized on the amide and the LUMO on the carbene and both are thus spatially decoupled, this molecular design minimizes the exchange energy between emissive intramolecular charge-transfer (CT) states and promotes efficient reverse ISC (rISC) between singlet and triplet states of CT character.[9,10] The computations on gold-centered CMAs have indicated a direct ^{1}CT–^{3}CT pathway enabled by strong SOC from the metal bridge. Conversely, the presence of a nearby locally excited triplet state (^{3}LE) slows down emission kinetics.[9,10] This finding contrasts with one of the current interpretations of emission in organic TADF materials[21,22] where it has been proposed that

A.-P. M. Reponen, D. Credgington, N. C. Greenham
Cavendish Laboratory
Department of Physics
University of Cambridge
J J Thomson Avenue, Cambridge CB3 0HE, UK
E-mail: ncg11@cam.ac.uk

The ORCID identification number(s) for the author(s) of this article can be found under https://doi.org/10.1002/adom.202200312.

DOI: 10.1002/adom.202200312

F. Chotard, M. Bochmann, A. S. Romanov
School of Chemistry
University of East Anglia
Earlham Road, Norwich NR4 7TJ, UK
E-mail: alexander.romanov@manchester.ac.uk

A. Lempelto, V. Shekhovtsev, M. Linnolahti
Department of Chemistry
University of Eastern Finland
Joensuu Campus, Joensuu FI-80101, Finland
E-mail: mikko.linnolahti@uef.fi

A. S. Romanov
Department of Chemistry
University of Manchester
Manchester M13 9PL, UK

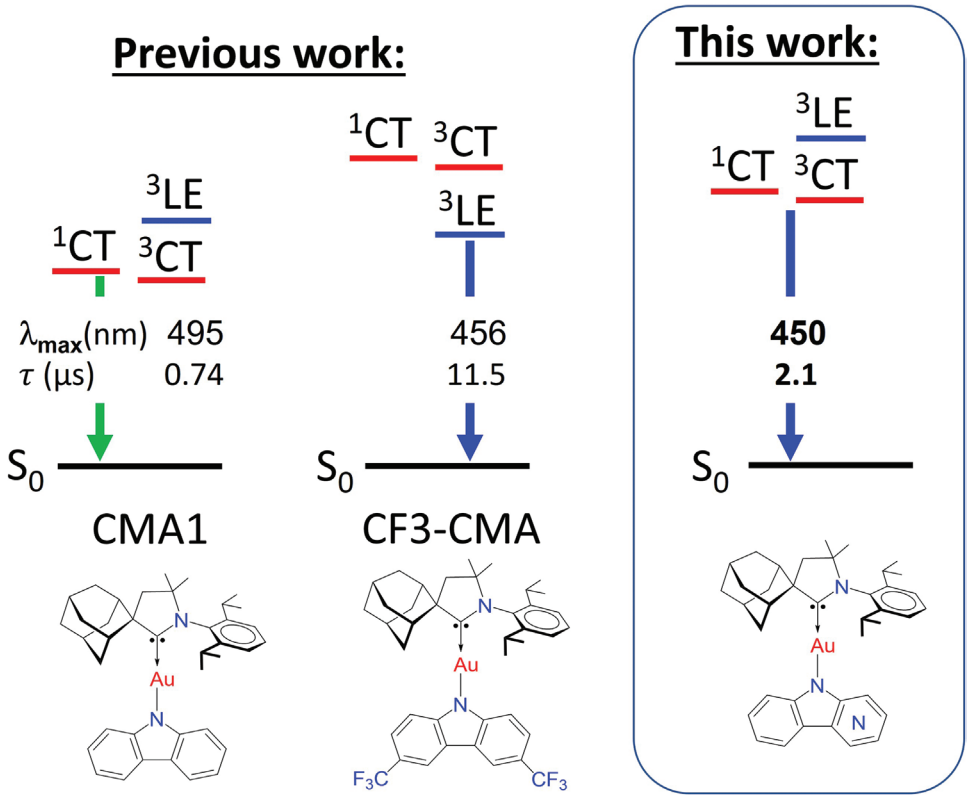

Figure 1. Left: schematic energy diagram and structure of the benchmark materials CMA1 and a blue variant CF3-CMA where ^{3}LE phosphorescence is observed. Right: aza-concept for fast and deep-blue CMA materials.

conversion between ^{1}CT and ^{3}CT states requires involvement of a ^{3}LE state[23–25] ideally resonant with the manifold of the CT states.[26]

Evidence for the impact of interactions between CT and ^{3}LE states in these donor–acceptor complexes comes from both environmental effects and chemical substitution. Previous works[27] demonstrate that the CT-LE gap in the gold-centred CMA1 material (**Figure 1**, left) can be tuned experimentally via environmental polarity effects in solid films. This is achieved by shifting the CT emission, as the LE state energy is less sensitive to the polarity of the environment.[27] A slight increase in emission lifetime is seen as CT emission increases in energy and approaches the energy of the ^{3}LE state. This is consistent with theoretical results indicating that a higher-lying ^{3}LE state is not able to mediate emission in a beneficial manner for CMA materials.[11,27] Fast emission in CMAs is then suggested to be achievable by reducing the contribution from ^{3}LE states and further minimizing the ^{1}CT–^{3}CT gap.

Chemical modification of the donor group in gold-centered CMAs also points to the same structure–property relationship between the electronic properties of the substituents and the emission behavior across the whole visible range.[14] For instance, increasing the number of electron-withdrawing CF_3 groups attached to the carbazole-donor (Figure 1) stabilizes the HOMO and blueshifts the CT emission. However, OLED devices made from a series of such modified CMA variants show the limitations of this approach due to decreased operational device lifetimes which correlates with increase of the emission lifetime while the emission blue-shifts for CMA material.[4–6] The doubly-substituted blue CF_3-CMA material shown in Figure 1 possesses a relatively long emission lifetimes of up to 11.5 µs, comparable to organic TADF emitters. Such slow emission is linked to the ^{3}LE state having a lower energy than the manifold of the CT states. This results in a significant contribution from ^{3}LE phosphorescence.[4–6] Long triplet lifetimes are especially problematic for the realization of deep-blue OLEDs with long operating device stability due to susceptibility to bimolecular annihilation reactions.[28,29] There is therefore a need to understand how to engineer materials with short excited state lifetimes for applications in deep-blue OLEDs.

While environmental effects[11,27] and chemical substitution[4–6,14] described above have been employed to shift the CT–^{3}LE gap in CMAs, these usually focus on shifting the CT state energy, such that their ^{3}LE states still present an upper limit for the energy of efficient and fast CT emission. In this work we present an alternative molecular design approach, which aims to achieve simultaneous control of both the lowest CT and ^{3}LE states, thereby allowing direct control of the CT–^{3}LE energy gap and a means to avoid population of ^{3}LE states (Figure 1).

We focused our attention on azacarbazoles as donor ligands. Azacarbazoles (pyridoindoles, or carbolines) are a class of organic molecules where a π-deficient pyridine ring is fused with a π-rich indole ring.[30] These ligands allow tuning the electron donor property by altering the position and number of N-atoms in the azacarbazole moiety to effectively manage the charge transport properties of host materials[31,32] or modulate

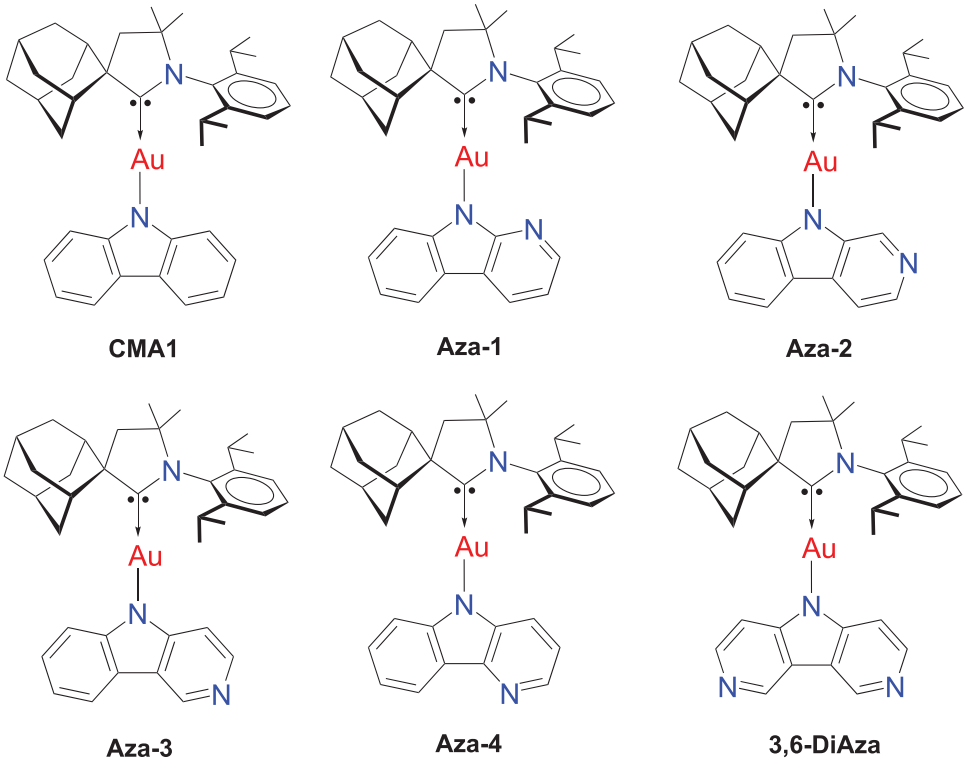

Figure 2. Structures of CMA1 and its Aza-substituted derivatives.

the triplet (T_1) energy level and bandgap of TADF materials.[33] Here, we have synthesized and investigated the luminescence behavior of a series of linear gold CMA complexes with various azacarbazole ligands (**Figure 2**) and compared those with CMA1 (Figure 1a), a well-investigated[1–6,9–12,27,34,35] gold-centered CMA with a carbazole donor, as a benchmark material.

We find that the extent to which CT and ^{3}LE states are shifted relative to CMA1 varies with the position of the substituted nitrogen atom. CT states are blueshifted in all cases. The value of this blueshift depends on the extent of HOMO stabilization and the position of the substitution. We demonstrate that the ^{3}LE states can be blueshifted or redshifted depending on how the substitution stabilizes relevant orbitals. As a result, the CT–^{3}LE gap varies within the series and is not solely dependent on the CT energy. This allows for blueshifting of CT emission while maintaining a higher-lying ^{3}LE state.

2. Results and Discussion

All complexes (Figure 2) were prepared by reacting (^{Ad}CAAC)AuCl with various donor ligands: 1-azacarbazole (Aza-1), 2-azacarbazole (Aza-2), 3-azacarbazole (Aza-3), 4-azacarbazole (Aza-4), or 3,6-diazacarbazole (3,6-DiAza), following our previously published methods.[1,12] All complexes have been characterized by ^{1}H and ^{13}C{^{1}H} NMR spectroscopy, high-resolution mass spectrometry and elemental analysis. All complexes have high solubility in THF, DCM, 1,2-difluorobenzene, and toluene and are sparingly soluble in hexanes. To estimate HOMO and LUMO energy levels we measured cyclic voltammetry in THF solution (Table S13, Figure S11, Supporting Information with ferrocene/ferrocenium (Fc/Fc+) redox couple as a reference). All complexes demonstrate quasi-reversible reduction and irreversible oxidation processes. The Aza1-4 complexes show small variations in reduction $E_{1/2}$ values (−2.74 ± 0.03 V) resulting in very similar LUMO energy levels (−2.73 ± 0.02 eV) whereas 3,6-Diaza exhibits a reduction $E_{1/2}$ value of −2.65 V and the LUMO is destabilized by 0.1 eV compared with mono-aza complexes. The oxidation process is centered on the azacarbazole ligand, with very similar E_p values at +0.57 ± 0.01 V for Aza-1 and Aza-3 complexes while measured at +0.48 ± 0.01 V for Aza-2 and Aza-4 complexes, in line with the increasing electron-donor effect of the nitrogen position in the azacarbazole. These results indicate that Aza-1 and Aza-3 carbazoles are less efficient electron donors in CMA complexes than Aza-2 and Aza-4 carbazoles.[36] The 3,6-Diaza complex shows the highest oxidation potential, with an E_p value of +1.04 V, which is expected due to presence of two π-deficient pyridine rings, thus indicating that the 3,6-diazacarbazole moiety is the weakest electron donor in the CMA series. The resulting HOMO energy values and bandgaps increase in the order CMA1 (−5.61 eV),[1] Aza-2 and Aza-4 (−5.74 eV), Aza-1 and Aza-3 (−5.81 eV), and 3,6-Diaza (−6.22 eV, Table S13, Supporting Information).

2.1. Photophysical Properties in Toluene Solution

CMA1 and aza-derivatives were investigated in 0.5 mg mL^{-1} toluene solutions. The data are collected in **Table 1**. The absorption spectra show the lowest-energy features as a broad CT peak

Table 1. Key photophysical properties of CMA1 and the aza-derivatives in various environments.

	λ_{em} [nm]	τ [µs][b)]	Φ [%, N_2][c)]	k_r [10^5 s^{-1}][d)]	k_{nr} [10^5 s^{-1}][d)]	CT/^{3}LE onset [eV][e)]	ΔE(CT–^{3}LE) [meV]	τ_{ISC} [ps][f)]	k_{ISC} [10^9 s^{-1}]
3% PS matrix[a)], 293 K									
CMA1	498	1.2	73	6.1	2.3	2.86/–	–	9	110
Aza-1	449	–	23	–	–	Mixed	–	6	170
Aza-2	478	–	27	–	–	Mixed	–	6	170
Aza-3	450	2.1	66	3.1	1.6	3.08/–	–	7	140
Aza-4	454	–	32	–	–	Mixed	–	6	170
3,6-DiAza	419	–	6	–	–	Mixed	–	3*	330*
Toluene, 293 K									
CMA1	528	1.2	95	7.9	0.42	2.7/–	–240	12	83
Aza-1	474	5.1	73	1.4	0.53	3.00/–	90	15	67
Aza-2	500	1.9	95	5.0	0.26	2.86/–	70	13	77
Aza-3	486	0.8	61	7.6	4.9	2.95/–	–90	12	83
Aza-4	506	1.7	100	5.9	–	2.84/–	30	11	91
3,6-DiAza	433	3.2	16	0.5	2.6	3.26/–	70	4*	250*
MeTHF, 77 K									
CMA1	426	302	–	–	–	–/2.95	–	–	–
Aza-1	431	3910	–	–	–	–/2.91	–	–	–
Aza-2	456	3019	–	–	–	–/2.79	–	–	–
Aza-3	413	1490	–	–	–	–/3.04	–	–	–
Aza-4	457	1527	–	–	–	–/2.80	–	–	–
3,6-DiAza	417	11 830	–	–	–	–/3.19	–	–	–

[a)]Films were prepared by drop-casting from chlorobenzene solutions onto a quartz substrate at 80 °C and annealed for 10 min; [b)]For cases where the emission decay lifetime was similar to the laser repetition rate no timescale could be reliably extracted; [c)]Quantum yields determined using an integrating sphere with flowing nitrogen; [d)]Radiative rate constant $k_r = \Phi/\tau$ and nonradiative constant $k_{nr} = (1 - \Phi)/\tau$; [e)]^{1}CT and ^{3}LE energy levels based on the onset values of the emission spectra blue edge. In cases where mixed CT and LE emission is observed the onset is not estimated; [f)]ISC timescales were estimated from an exponential fit to the rise kinetic of the late-time excited-state absorption (ESA) edge, which has been assigned to the T_1 state.*For 3,6-DiAza no such rise kinetic is observed in the probed range so the fall kinetic of the early-time ESA is used instead. Notation: In this work, ^{1}CT and ^{3}CT refer to the lowest excited CT singlet and triplet states, respectively. ^{1}LE and ^{3}LE refer to the lowest excited singlet and triplet states localized on the amide donor unless otherwise mentioned.

which partially overlaps with a set of sharp peaks between 350 and 380 nm (**Figure 3**). This is attributed to π–π^* transitions localized on the donor ligand in line with previous investigations on CMA materials.[27,35] Sharp localized π–π^* transitions of the donor ligand are difficult to discern for Aza-1 complex and appear as a shoulder above 375 nm.

In toluene solution at 298 K all complexes show broad, unstructured emission peaks ascribed to CT processes (Figure 3). The luminescence profile is blueshifted by 20–90 nm in all aza-derivatives compared to CMA1. The extent of the blueshift (measured from the PL onset) is greatest for complexes Aza-1 and Aza-3 at 0.30 and 0.25 eV, respectively, and smaller for complexes Aza-2 and Aza-4 at 0.16 and 0.14 eV, respectively, in line with the trend in HOMO energy levels: CMA1 < Aza-2 and Aza-4 < Aza-1 and Aza-3, vide supra. The trend in PL emission energies with substitution location is the same as observed in a study of radical emitters with similar nitrogen-substituted carbazole donors.[37] In that report, the blueshift trend was related to the HOMO coefficient at the substitution site of the carbazole moiety.

Luminescence decay in toluene solution is monoexponential for all materials (Figure S8, Supporting Information), with emission lifetimes typically in the range of 0.8–1.9 µs, while Aza-1 is noticeably slower, with an emission lifetime of 5 µs. PLQY values in solution range from near unity for Aza-2 and Aza-4 to up to 71% for the Aza-1 and Aza-3 (Table 1).

3. Photophysical Properties of 3 wt% PS Films

Emissions in polystyrene (PS) hosted films are blueshifted compared to toluene solutions by about 0.1 eV at the CT peak, with a noticeably structured profile for all materials except CMA1 and Aza-3 (Figure 3, Table 1). Blueshifts of the CT emission for CMAs in dilute hosted films compared to solutions and neat amorphous films have been explored in our previous study of environmental effects on CMA1 emission properties.[27] It was explained that the emission in amorphous films arises from a non-equilibrium ensemble of triplet excited states. Only the low-energy tail of the density of states corresponds to molecules near the fully relaxed S_1 geometry, such that energetic relaxation requires diffusion toward these sites. At low CMA concentrations, the reduced effective diffusion rate leads to blueshifting of the time-averaged PL spectra. In polar environments there is

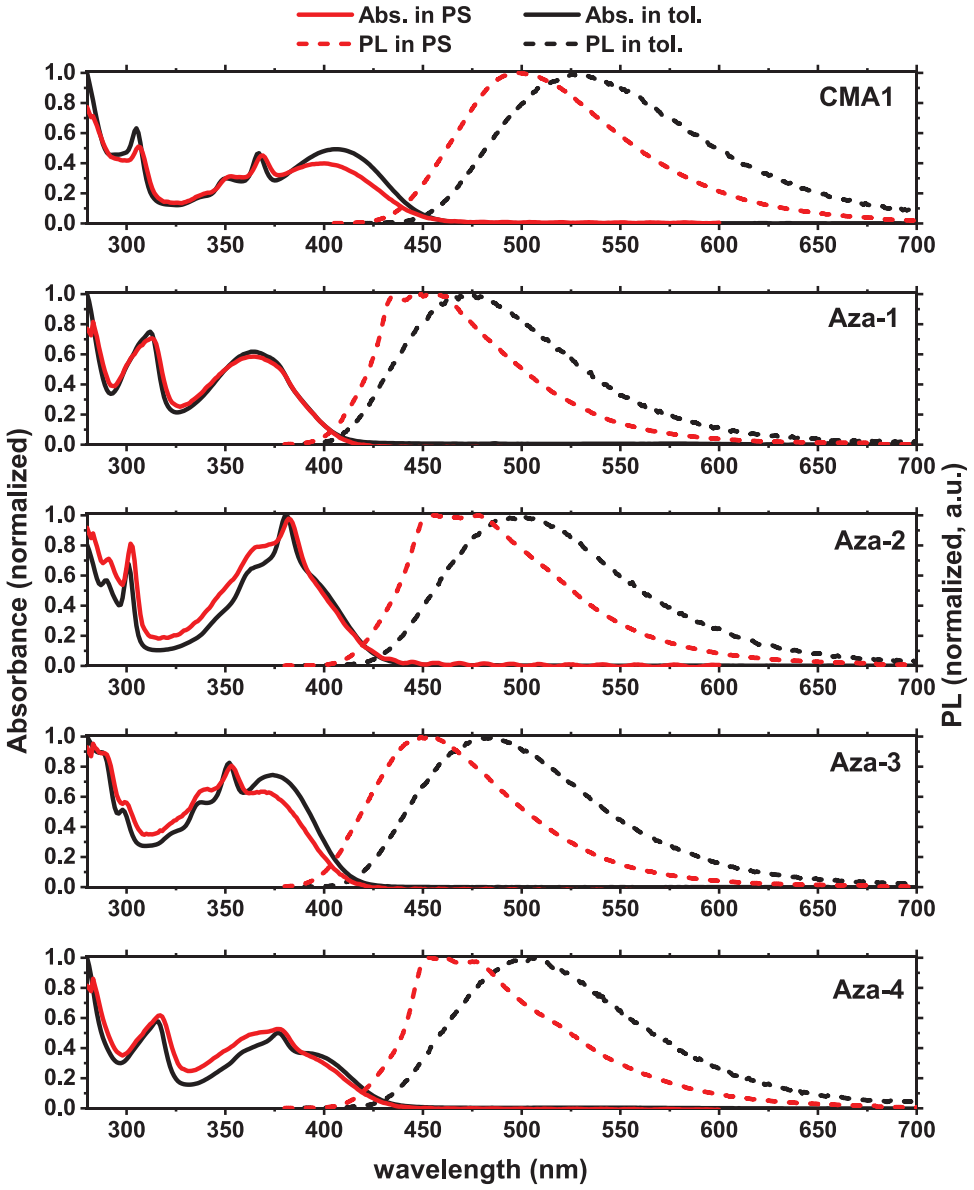

Figure 3. UV–vis absorption (solid lines) and photoluminescence (dashed lines) spectra for CMA1 and the aza-derivatives in toluene solution (black) and of drop-cast CMA:PS films at 3 wt% dopant level (red) under nitrogen.

an additional shift due to electrostatic interactions between the CMA and the environment.[27,38]

We attribute the structure of emission in some PS films to phosphorescence from a ^{3}LE state overlapping with the CT emission. To support this, we first compare the emission spectra of films in air and under flowing nitrogen (**Figure 4**). The triplet-quenching effect of atmospheric oxygen reduces both CT and ^{3}LE emission as both processes involve triplets, but ^{3}LE phosphoresence is more strongly affected due to its longer emission lifetime. By performing a weighted subtraction of these spectra, we can obtain an estimate of the spectrum of the species which is more air-sensitive. The PL in air shows less structure than under flowing nitrogen, indicating much greater sensitivity to oxygen quenching of the ^{3}LE state.

The difference spectra for Aza-1, Aza-2, and Aza-4 (Figure 4, blue line) in PS films are in good agreement with PL spectra measured in MeTHF at 77 K (**Figure 5**). In frozen MeTHF, the emission spectrum is heavily dominated by ^{3}LE phosphorescence. This is attributed to the rigid polar environment restricting structural relaxation and increasing CT state energy as described for CMAs in solid polar hosts,[38] along with the low temperature slowing down thermally activated steps in the emission process. The air–nitrogen difference spectra for CMA1 and Aza-3 complexes do not show any obvious structure and do not match with the ^{3}LE emission seen in frozen MeTHF, indicating that ^{3}LE emission does not occur at room temperature in PS hosted films of these materials.

The onset of phosphorescence is also seen in time-resolved photoluminescence data, where Aza-1, Aza-2, and Aza-4 show

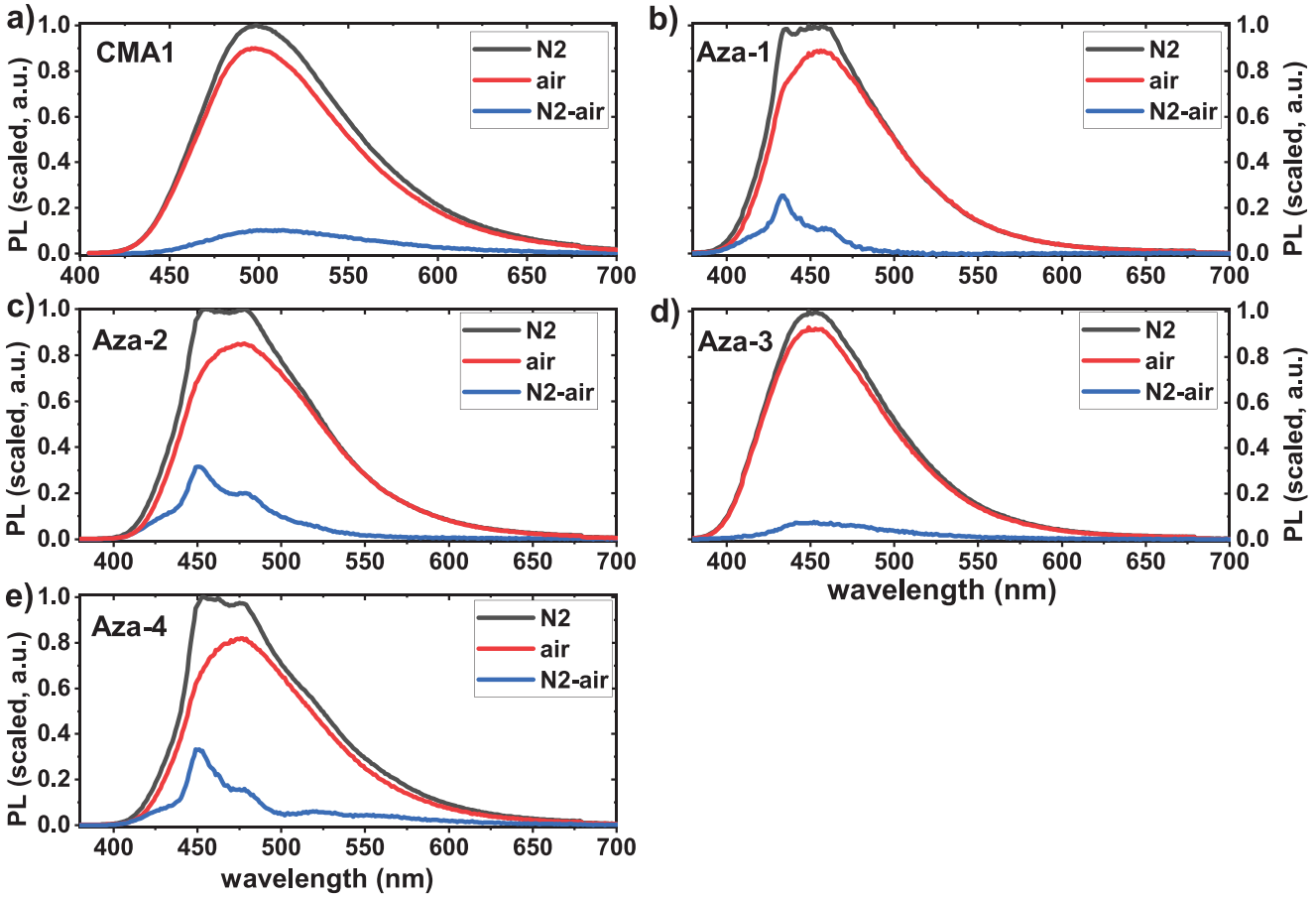

Figure 4. PL spectra of 3 wt% CMA:PS films measured under 370 nm excitation in air and under flowing nitrogen, rescaled for complexes CMA1 (a), Aza-1 (b), Aza-2 (c), Aza-3 (d), Aza-4 (e). The rescaled "air" spectrum is subtracted from the "nitrogen" spectrum to give a difference spectrum.

mostly unstructured CT-like emission up to about 1 µs, and strongly structured emission consistent with the presence of the ^{3}LE emission on longer timescales (**Figure 6**). The presence of ^{3}LE emission is accompanied by significantly reduced PLQYs compared to solutions (Table 1). In contrast, for CMA1 and Aza-3 emission is CT-like throughout and decays on 1–2 µs timescales with mostly monoexponential kinetics (Figure 6), similar to those observed in toluene solutions. PLQYs are similar or only slightly reduced compared to toluene solutions (73% for CMA1 and 66% for Aza-3, Table 1). This is again consistent with the lack of ^{3}LE phosphorescence in these materials.

The lack of ^{3}LE phosphorescence in Aza-3 is important as it has a relatively blue CT emission compared to other materials in the series (Table 1). As described above, strongly blue-shifting the CT energy usually makes CMAs more susceptible to unwanted ^{3}LE emission.[4–6] From PL spectra taken in MeTHF at 77K (Figure 5), we find that the ^{3}LE emission in Aza-3 has an onset at 3.04 eV. This is at a higher energy than the ^{3}LE emission onset of CMA1 at 2.95 eV (Table 1), whereas all other aza-derivatives have their ^{3}LE emission at a lower energy than CMA1, with a slight shift to 2.91 eV in Aza-1 and a more substantial one to 2.71 and 2.80 eV in Aza-2 and Aza-4, respectively (Table 1).

Based on this, and as hypothesized, it is apparent that the aza-substitutions can impact both the donor-centered ^{3}LE state energy and the energy of the CT state. This has important consequences for emission kinetics which depend on the relative energies of the CT and ^{3}LE states. Where the phosphorescent ^{3}LE state is blueshifted to lie above the CT states, CT emission is preserved. For example, despite the relatively large blueshift (compared to CMA1) of the CT state in Aza-3, emission remains CT-like and relatively fast due to the ^{3}LE state being blueshifted far enough to not be emissive even in solid films. In the other aza-derivatives ^{3}LE emission is actually redshifted compared to CMA1 while CT emission is blueshifted, resulting in ^{3}LE phosphorescence in the solid state and long emission lifetimes.

3.1. Computational Results

In order to link the changes seen in CT and LE state energies with the aza-substitution pattern, we characterized these excitations through computational methods. The lowest excited states are calculated first for vertical transitions in the ground-state S_0 geometry using time-dependent density functional theory (TD-DFT). The lowest singlet and triplet states (S_1 and T_1) are found to be CT states of predominantly HOMO → LUMO character (Table S6, Supporting Information). The second-lowest excited triplet (T_2) is in all cases found to be an LE state of predominantly HOMO → LUMO + 3 character localized on the

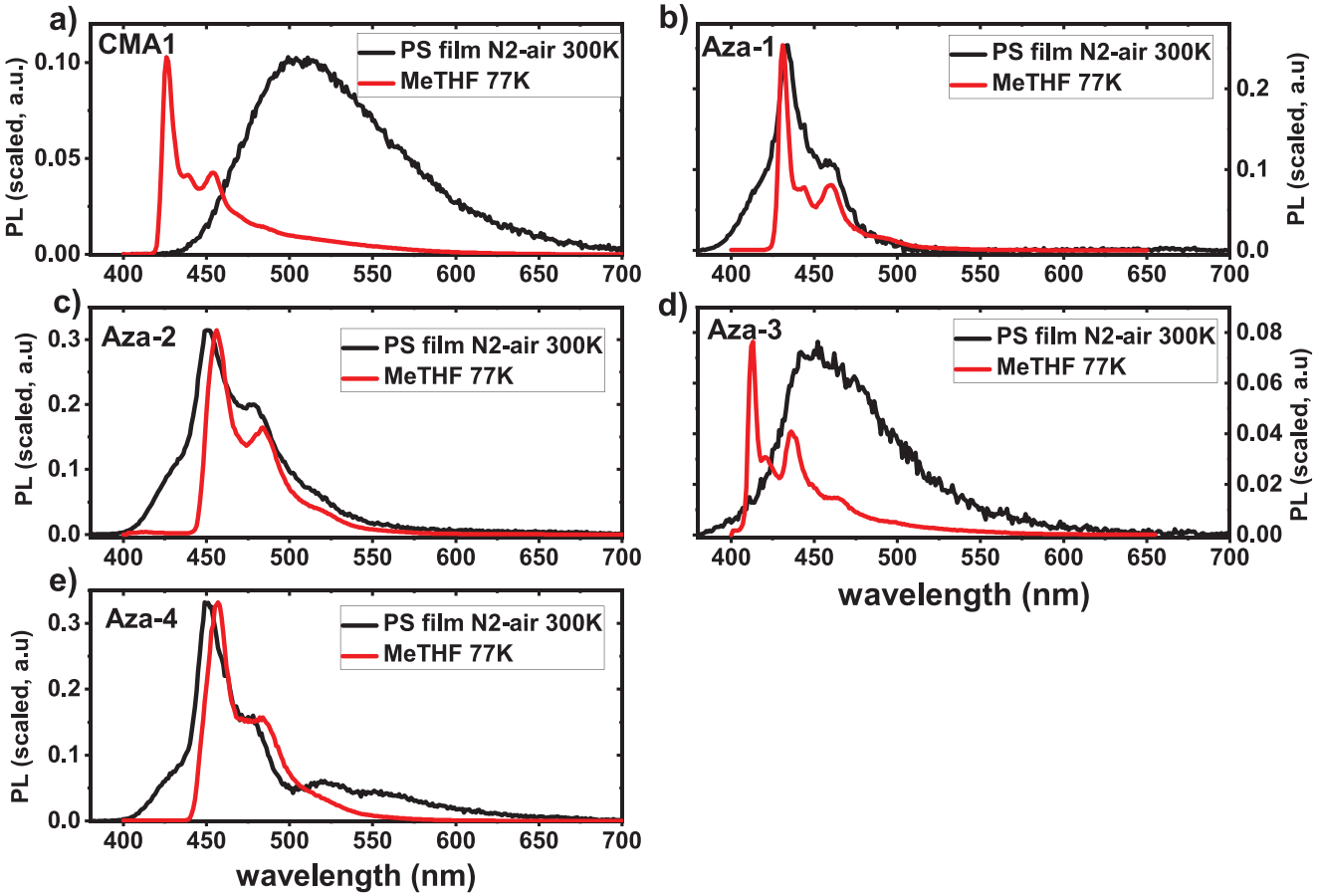

Figure 5. Weighted subtractions of the PL spectra in air and nitrogen for 3 wt% PS-hosted CMA films at room temperature (black lines) plotted along PL spectra in frozen MeTHF solutions (red lines) for CMA1 (a) and the aza-derivatives Aza-1 (b), Aza-2 (c), Aza-3 (d), Aza-4 (e).

carbazole-derivative donor (Table S7, Supporting Information). These orbitals retain much of their character between substituted variants, and are plotted in **Figure 7**.

Predicted energies of the ^{1}CT vertical transitions (**Table 2**) are well matched with experimental absorption spectra and reproduce the order of CT band blueshift. Geometry optimization has been carried out for S_1 and T_1 states with results presented in Table S10, Figure S11, Supporting Information. It is found that the optimum geometry for each state (S_0, S_1, and T_1) is different, with donor and acceptor being coplanar in S_0 and T_1 but orthogonal in S_1. For simplicity, we will focus on the ground-state geometry in the main text.

Next, we explore the effect of aza-substitution on the calculated frontier orbitals energy and aim to explain the experimentally observed relative energies of the excited states. Following a first-order perturbation theory approach outlined in another study,[37] the electron-withdrawing nitrogen substitution is expected to stabilize the donor-centered orbitals compared to the unsubstituted molecule, and the stabilizing effect is expected to be proportional to the orbital coefficient at the substitution location. At a coarser level, we would expect the orbital stabilization effect to be greater when the substitution is at an orbital wavefunction antinode, and smaller when located at an orbital wavefunction node. The isosurface plots in Figure 7 show that the aza-substitution locations are mostly near orbital nodes or antinodes. To quantify the involvement of each substitution site to a given orbital, we evaluated population of the substituted nitrogen atoms through Natural Population Analysis (NPA). These results are presented alongside calculated orbital energies in Table 2. To illustrate the link between these quantities, we have plotted the energy shifts of HOMO and LUMO + 3 orbitals against the substitution site population in **Figure 8**. We find that the donor-centered orbitals HOMO and LUMO + 3 are stabilized in all aza-derivatives compared to CMA1, as expected. The materials are clustered at the corners of the figures, with the top-left corner containing Aza-2 and Aza-4 which have their aza-substitution sites at the meta-position with little population of the HOMO orbital and subsequently show smaller stabilization of the HOMO. For the Aza-3, the same is true for the LUMO + 3 orbital. The bottom-right corner contains materials where aza-substitution site population and energetic stabilization are larger. We can distinguish between the materials which are more stabilized or less stabilized for both of the donor-centered HOMO and LUMO + 3 orbitals. It appeared that complex Aza-3 is the only complex having the least stabilization of the LUMO + 3 (associated with the ^{3}LE) which provides an explaination for the significant blue shift of the ^{3}LE luminescence (Tables 1,2).

To compare computational and experimental results, we measure characteristic state energies from the high-energy

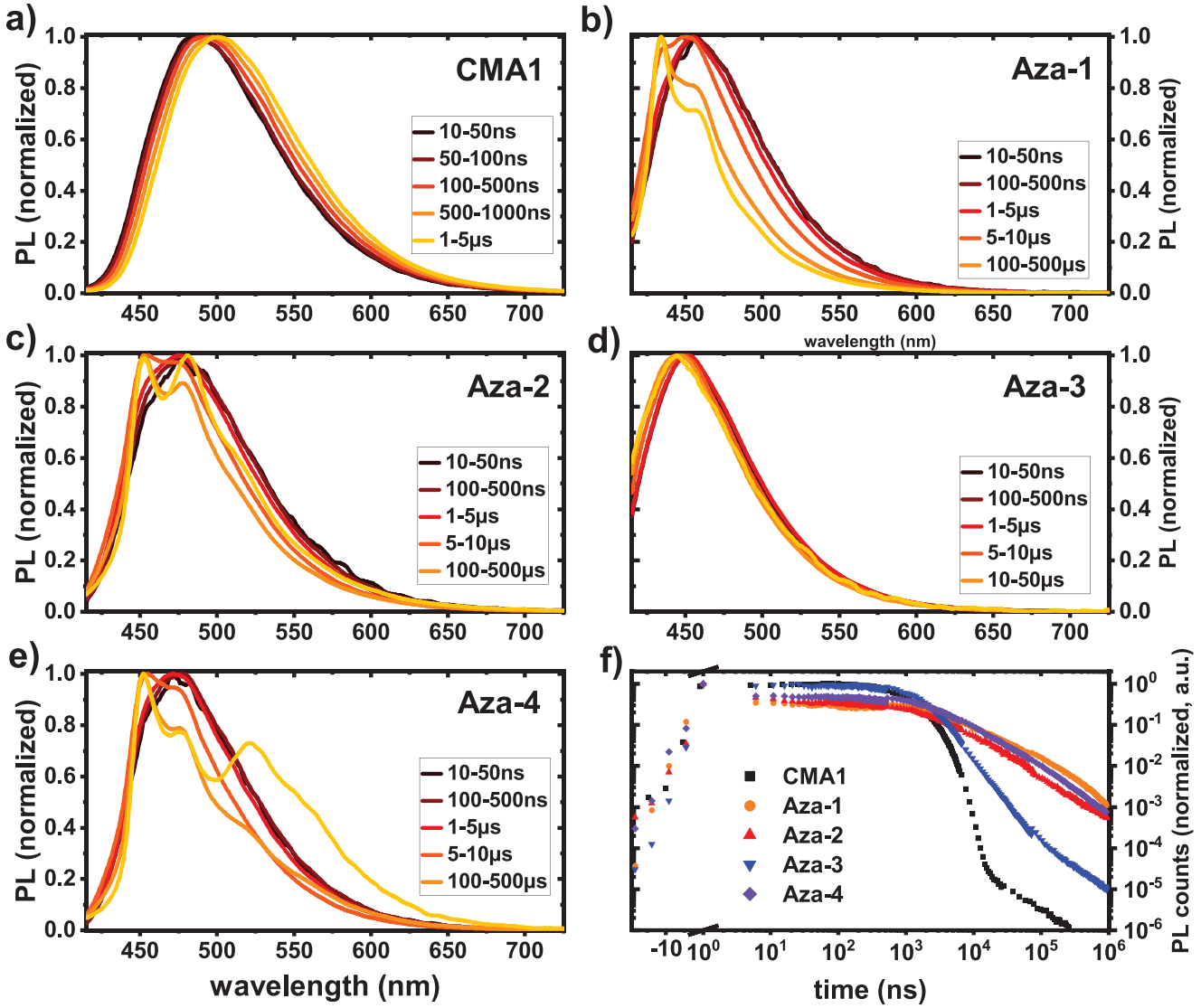

Figure 6. a–e) Time-resolved normalized emission spectra of the aza-derivatives in 3 wt% PS hosted films. f) Time-resolved emission kinetics (integrated over the emission range) for aza-derivatives in 3 wt% PS hosted films. Excitation at 372 nm, samples were held in a vacuum.

onset of emission to estimate of the relevant state[39,40] and the energy splitting between ^{1}CT and ^{3}LE states.[41] We plot the onset energies along with the energies of the discussed orbitals ($E_{LUMO+3} - E_{HOMO}$ for ^{3}LE states and $-E_{HOMO}$ for CT states as the LUMO is localized on the acceptor) in **Figure 9**. Both data series for CT and ^{3}LE states indicate that the variation in emission energies is directly connected with changes in the orbital energies and correlates with the position of the N-atom in the carbazole moiety. This allows us to explicitly describe the reason for the relative state energies of CT and ^{3}LE states in the aza-derivatives compared to CMA1. Looking at the key orbitals in Figure 7, we see that the HOMO is mostly located on the donor and the LUMO mostly located on the acceptor. Aza-1 and Aza-3 complexes have nitrogen substitutions close to the HOMO antinodes (Figure 7). This stabilizes the HOMO by about 0.3 eV (Figure 8) which strongly blueshifts the CT states (HOMO → LUMO) compared to CMA1 (Figure 9). For Aza-2 and Aza-4 the substitutions are near the edge of HOMO nodes, so the HOMO orbitals are stabilized less (by about 0.2 eV, Figure 8) and subsequently CT states are blueshifted less (Figure 9). This explains why CT emission is bluer for Aza-1 and Aza-3 than Aza-2 and Aza-4.

The LUMO + 3 orbital involved in the ^{3}LE state (HOMO → LUMO + 3) has an antinode at the substitution site for all materials except Aza-3 (Figure 7). As a consequence, the LUMO + 3 is only stabilized by about 0.1 eV for Aza-3 but significantly more stabilized (about 0.3 eV) for all other complexes (Figure 8). As the HOMO is stabilized by 0.3 eV for Aza-3, the ^{3}LE state is then higher in energy compared to CMA1 (Figure 9). All other aza-derivatives have a LUMO + 3 stabilized by a similar (Aza-1) or greater (Aza-2 and Aza-4) amount than the HOMO, resulting in the ^{3}LE states being similar (Aza-1) or lower (Aza-2 and Aza-4) in energy than for CMA1 (Figure 9). This explains why Aza-3 is the only aza-derivative to show a blueshifted ^{3}LE state compared to CMA1.

These results suggest an aza-substitution in para-position for the pyrrole N-atom of the carbazole in CMA materials can

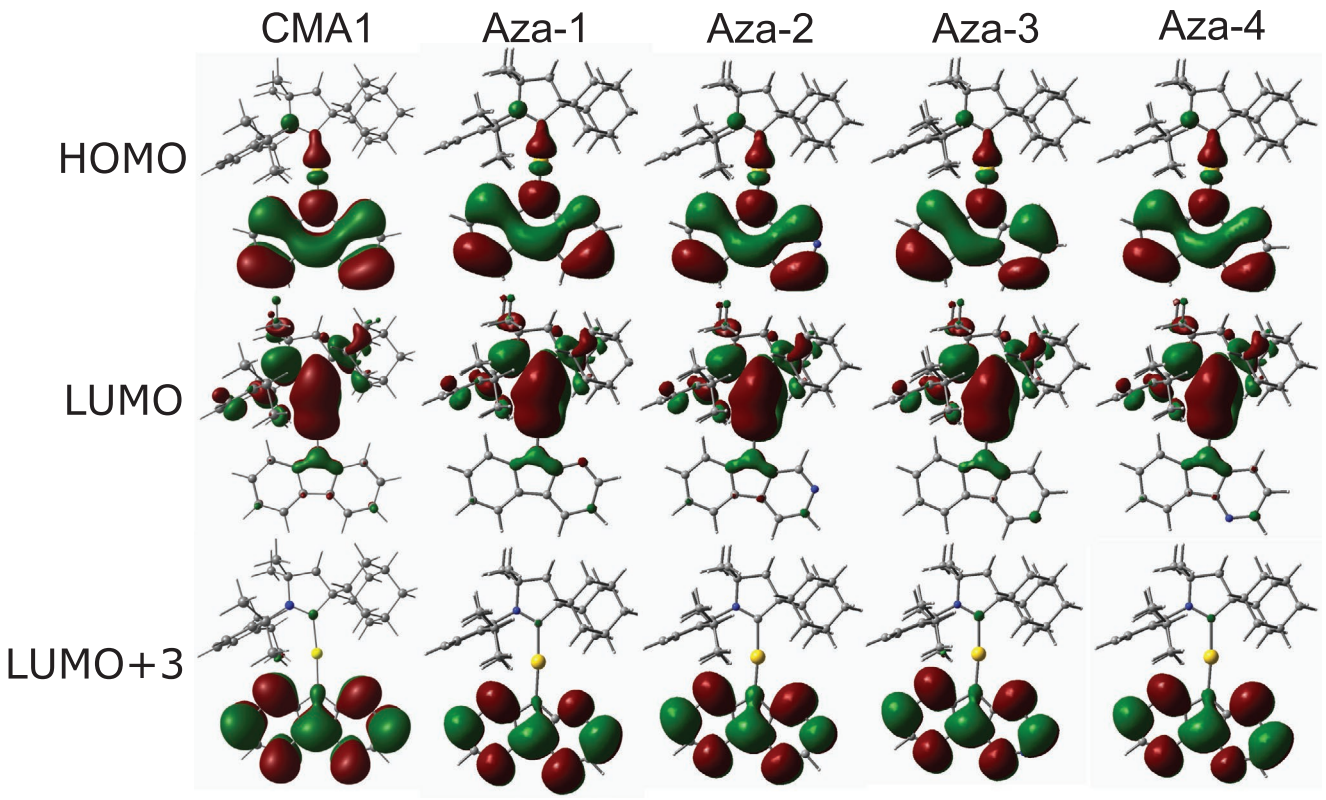

Figure 7. Isosurface plots of the main orbitals involved in the lowest excited singlet ^{1}CT (HOMO → LUMO), and the two lowest excited triplets, ^{3}CT (HOMO → LUMO) and ^{3}LE (HOMO → LUMO + 3) for CMA1 and the aza-derivatives.

be used as a reliable approach to simultaneously tune the energies of LE and CT states. We have employed this strategy to achieve blue CT luminescence while avoiding undesirable ^{3}LE emission with successful demonstration on the Aza-3 complex, which shows the desired deep-blue CT luminescence (CIE 0.16; 0.18) without slow ^{3}LE emission in a PS matrix.

3.2. Linking CT–^{3}LE Gap to Radiative Decay Rates

The presence of a lower-lying 3LE state is clearly detrimental for emission in solid state, leading to parasitic ^{3}LE phosphorescence and mixed CT/LE emission. We next consider the impact on emission in solution, where phosphorescence is typically not observed and rapid geometric relaxation in the excited state can occur,[1] such that only CT emission is visible. We estimate the CT and the ^{3}LE states energies from the solution emission onsets as previously and plot the CT–^{3}LE energy gap against radiative decay rate as shown in **Figure 10**. The plot in Figure 10 shows that the radiative decay slows down as the CT–^{3}LE gap becomes more positive (i.e., ^{3}LE drops below CT). CMA1 and Aza-3 in toluene correspond to the schematic depicted in **Figure 11**a, with a relatively large and negative CT–^{3}LE gap that has little effect on the emission lifetime. This is similar to previously reported in studies of environmental effects on CMA1, which found a reduction in CT–^{3}LE gap to be associated with a small increase in emission lifetime.[11,27] For Aza-1, Aza-2, and Aza-4 in toluene, the situation corresponds to Figure 11b,

Table 2. Calculated energies of the lowest excited states and the main orbitals involved in ground-state geometries for CMA1 and the aza-derivatives. NPA refers to the atomic population at the substitution site for the given orbitals as evaluated by Natural Population Analysis.

Molecule	E_{HOMO} [eV]	E_{LUMO} [eV]	E_{LUMO+3} [eV]	E_{1CT} [eV]	E_{3CT} [eV]	E_{3LE} [eV]	NPA (HOMO) [%]	NPA (LUMO + 3) [%]
CMA1	−5.43	−1.14	0.31	3.07	2.78	3.34	–	–
Aza-1	−5.74	−1.02	−0.05	3.40	3.10	3.32	6.6	11.3
Aza–2	−5.62	−1.17	0.00	3.19	2.90	3.18	0.1	11.8
Aza-3	−5.79	−1.26	0.19	3.29	3.01	3.53	6.3	0.4
Aza-4	−5.62	−1.23	0.04	3.17	2.86	3.22	1.6	15.3
3,6-DiAza	−6.24	−1.38	0.05	3.56	3.28	3.65	–	–

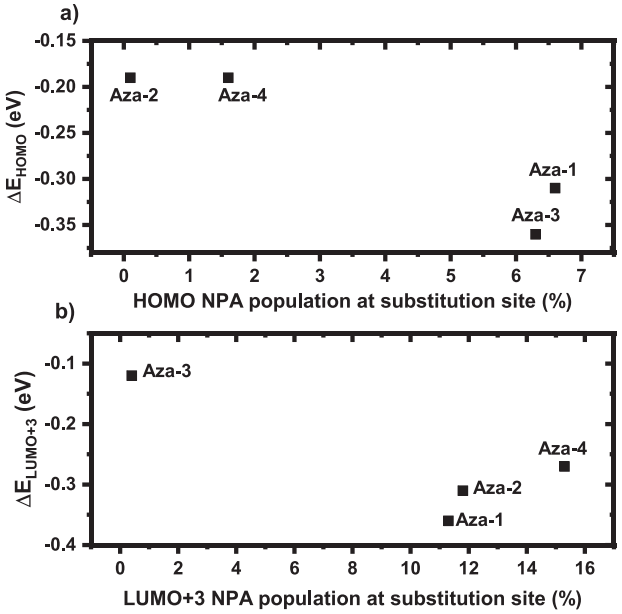

Figure 8. Atomic population at the substituted nitrogen for the given orbital as calculated by Natural Population Analysis for a) the HOMO and b) the LUMO + 3 orbitals, and calculated energy shifts of these orbitals relative to the unsubstituted variant CMA1.

where the ^{3}LE state is below the CT states resulting in slower rISC rates, possibly due to an additional energy barrier required to reach the CT states from a lower-lying ^{3}LE. Note, that in solution the ^{3}LE phosphorescence is not observed at room temperature.

The observed trends in aza-derivatized CMAs are consistent with an emission process that is not mediated by a triplet state lying energetically above ^{3}CT. This is in line with theoretical calculations and earlier works which propose emission occurring primarily by direct ^{1}CT–^{3}CT coupling, and for which the presence of a nearby ^{3}LE states is detrimental to the emission rate.[9–11] Overall, these results indicate that keeping the donor-^{3}LE states well above the CT states provides a reliable strategy for maintaining fast CT emission in gold-centered CMAs.

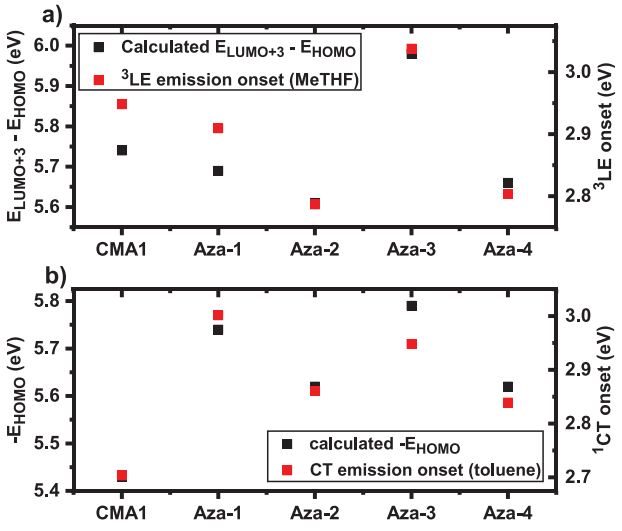

Figure 9. a) A comparison of the experimental PL onset energies for ^{3}LE emission in 77 K MeTHF and calculated LUMO + 3–HOMO energy gap. b) A comparison of the experimental PL onset energies for CT emission in toluene solution and the calculated HOMO energy.

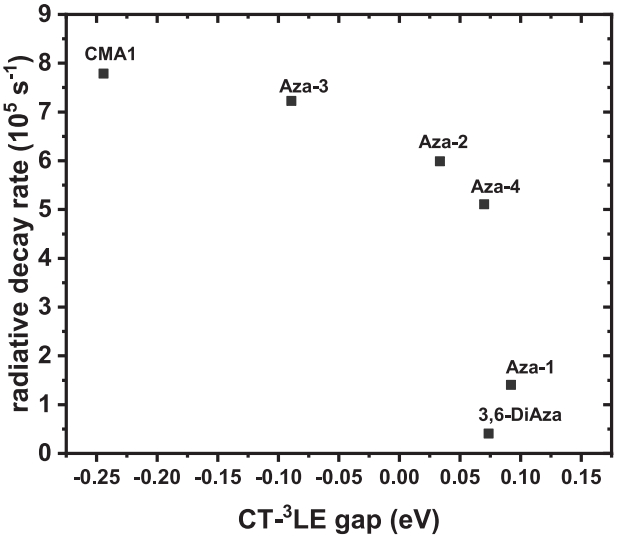

Figure 10. The CT–^{3}LE gap as determined from experimental emission spectrum onset energies versus radiative decay rate (PLQY corrected PL decay rate) for CMA1 and the aza-derivatives in toluene solution.

3.3. Transient Absorption

In order to understand how the CT–^{3}LE energy gap impacts the emission process, we performed transient absorption (TA) spectroscopy on all aza-derivatives and CMA1 to investigate variations in the rate of ISC from the lowest excited singlet state S_1 to the lowest triplet state T_1. A summary of timescales for the materials in various environments are summarized in **Table 3** with full spectroscopic data provided in Supporting Information (Figures S1,S2, Supporting Information for spectra, Figures S3–S6, Supporting Information for kinetics). Representative TA spectra on ps–ns pump–probe delay timescales

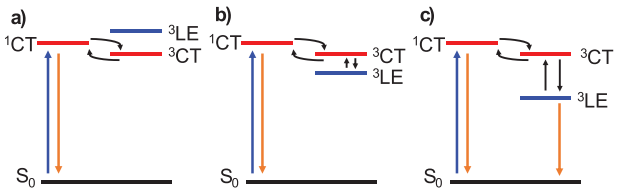

Figure 11. Schematic energy diagrams of the relevant states and couplings for the aza-derivatives in three regimes defined by relative energies of ^{3}LE and CT states. a) ^{3}LE is above the CT states. Emission rate and forward ISC do not strongly depend on ^{3}LE proximity to CT, indicating that the state does not mediate either of these processes. b) ^{3}LE state is below but near the CT states. Triplet ESAs change and emission slows down from slower rISC to ^{1}CT, possibly by an increased activation energy, but emission remains CT-like. c) ^{3}LE state is well below the CT states. CT emission mediated by rISC becomes slow, and long-lived ^{3}LE emission is observed.

Table 3. Transient absorption data for aza-derivatives, with estimated CT–^{3}LE gaps shown for reference. The late-time ESA peak locations are shown (rounded for easier comparison), and where two ESA peaks are present, the stronger one is bolded.

	0.5 mg mL^{-1} Toluene solution				3 wt% PS host film			
	CT–^{3}LE gap [eV]	Late-time ESA [nm]	Triplet ESA growth [ps]	Singlet ESA decay [ps]	CT–^{3}LE gap [eV]	Late-time ESA [nm]	Triplet ESA growth [ps]	Singlet ESA decay [ps]
CMA1	–0.24	600, **650**	12	5	–0.09	600, **650**	9	9
Aza-1	0.09	600	15	9	>0.09*	600	6	7
Aza-2	0.07	**600**, 650	13	4	>0.07*	600	6	7
Aza-3	–0.09	600, **650**	12	4	0.05	**600**, 650	7	7
Aza-4	0.03	550, **600**	11	3	>0.03*	550	6	5

*Due to the presence of simultaneous CT and 3LE emission, estimating a CT–^{3}LE gap from emission onset energies is not attempted; based on effects seen in CMA1 and Aza-3, it is assumed that the gap is larger in PS relative to toluene.

are plotted in **Figure 12** for CMA1 in PS matrix, and toluene solutions of Aza-2 and Aza-1.

All complexes show a conversion from an early-time species, which is populated immediately upon photoexcitation, to a late-time species, with the early-time species decaying on a timescale of 3–9 ps (Table 3). In previous reports for CMA1, these early and late species are assigned to S_1 and T_1, respectively.[1,21] For PS hosted films, kinetics assigned to singlet excited state absorption (ESA) decay and triplet ESA growth result in very similar timescales (Table 3). For toluene solutions, the decay kinetics of the singlet ESA feature is faster than the growth kinetics assigned to the triplet feature. Previous TA investigation of CMA1 complex in toluene solution noted kinetics as being relatively complex, with steps attributed to ISC and various relaxation processes.[34] In this work, we estimate characteristic timescales for ISC from triplet rise kinetics. In PS hosted films, all singly substituted aza-derivatives have ISC timescales of 6–7 ps, slightly faster than CMA1 (9 ps). The ISC timescale of CMA1 in toluene is estimated at 12 ps, which is similar to all other aza-CMA's (11–13 ps, Table 3). Only Aza-1 is notably different by having a slower ISC rate of 15 ps. We find no correlation between the measured ISC rates and the estimated CT–^{3}LE gap.

Based on the emission data (see Figure 5), we suggest that the character of the lowest-lying triplet T_1 changes from ^{3}CT to ^{3}LE across the aza-derivatives. Accordingly, we see a change in the late-time ESA spectra across materials and environments. ESA spectra assigned to T_1 generally show a peak/shoulder around 600 nm and a peak/shoulder around 650 nm (Figure 12, Table 3; Figures S1,S2, Supporting Information) with varied relative strengths.

From Table 3, we find that the 650 nm feature is dominant when the CT–^{3}LE gap is negative, for instance, CMA1 and Aza-3 in toluene or CMA1 in PS. The 650 nm feature is entirely absent when the CT–^{3}LE gap is positive and the emission has a prominent ^{3}LE component (Aza-1 and Aza-2 in PS) or retains CT character but is relatively slow (Aza-1 in toluene). Both 600 and 650 nm features are present, with the 600 nm feature slightly more prominent, where the CT–^{3}LE gap is estimated to be slightly positive but emission remains CT-like and has not greatly slowed down (Aza-2 in toluene and Aza-3 in PS). The trend is summarized in Figure 12, with examples of ESAs and schematics of the estimated relative state energies. Note that Aza-4 behaves similarly, however, the ESAs profiles are shifted by about 50 nm, peaking at 600 nm in toluene and 550 nm in PS.

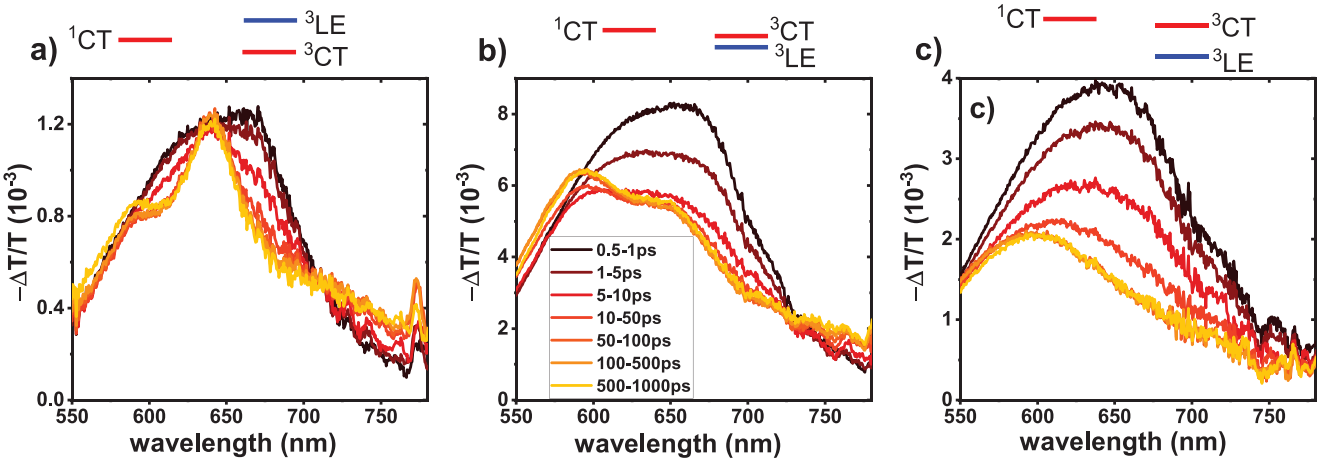

Figure 12. Transient absorption spectra showing the early-to-late species transition in CMA1 and aza-derivatives, as well as the change in late-time ESA shape between materials associated with a change in the lowest triplet character as illustrated by the schematics above the graphs. The legend indicates pump-probe delay. a) CMA1 in PS matrix, b) Aza-2 in toluene, and c) Aza-1 in toluene.

It seems plausible to link the appearance of the 650 nm late-time ESA peak to population of the ^{3}CT state. What we then see in the ESA variations is the ^{3}CT state becoming decreasingly populated as ^{3}LE is brought closer to and eventually below it, corresponding to a slower CT emission process and eventual onset of ^{3}LE phosphorescence. ISC timescales do not seem to be correlated with the proximity of the ^{3}LE and CT states, indicating that the ^{3}LE state is not crucial for mediating the ISC process from ^{1}CT. The overall mechanism for the trends and regimes seen in the aza-derivatives is summarized by Figure 11, accounting for effects seen in timescales and spectra associated with emission and ISC processes.

To explore longer-time kinetics, TA experiments with ns-ms pump-probe delays were carried out for the materials exhibiting ^{3}LE emission in PS hosted films. These show little evolution in the ESA shape over longer times. Profiles are collected in Figure S7, Supporting Information. The exception is Aza-4, where additional structure appears on timescales which can be correlated with the unusual late-time luminescence presented in Figure 6e.

3.4. Extension to a Double-Substituted CMA

Motivated by simultaneous blueshift of the CT and ^{3}LE states in Aza-3, we synthesized a gold complex 3,6-DiAza (see Figure 2) with two nitrogen substitutions in para-positions to the carbazole N-atom. We consider 3,6-DiAza separately from mono-aza variants due to the strongly blue-shifted UV–vis absorption edge (below 400 nm) which significantly increases experimental complexity. The 3,6-DiAza complex shows a CT emission peak at 433 nm in toluene (**Figure 13**a) which is up to 73 nm blue-shifted compared to singly substituted aza-derivatives (Table 1). The onset of the CT emission in toluene is measured at 3.26 eV, which is 0.56 eV higher than unsubstituted CMA1 and 0.26 eV higher than Aza-1, the bluest singly substituted aza-variant (Table 1). The emission in PS hosted films is structured (see Figure 13a), while the difference emission spectrum (PL under nitrogen minus PL in air) reveals a clear vibronic structure (Figure 13b). This is similar to what we observed for the singly substituted variants where the resultant difference spectra are mostly carbazole ^{3}LE emission, as is seen in MeTHF at 77 K

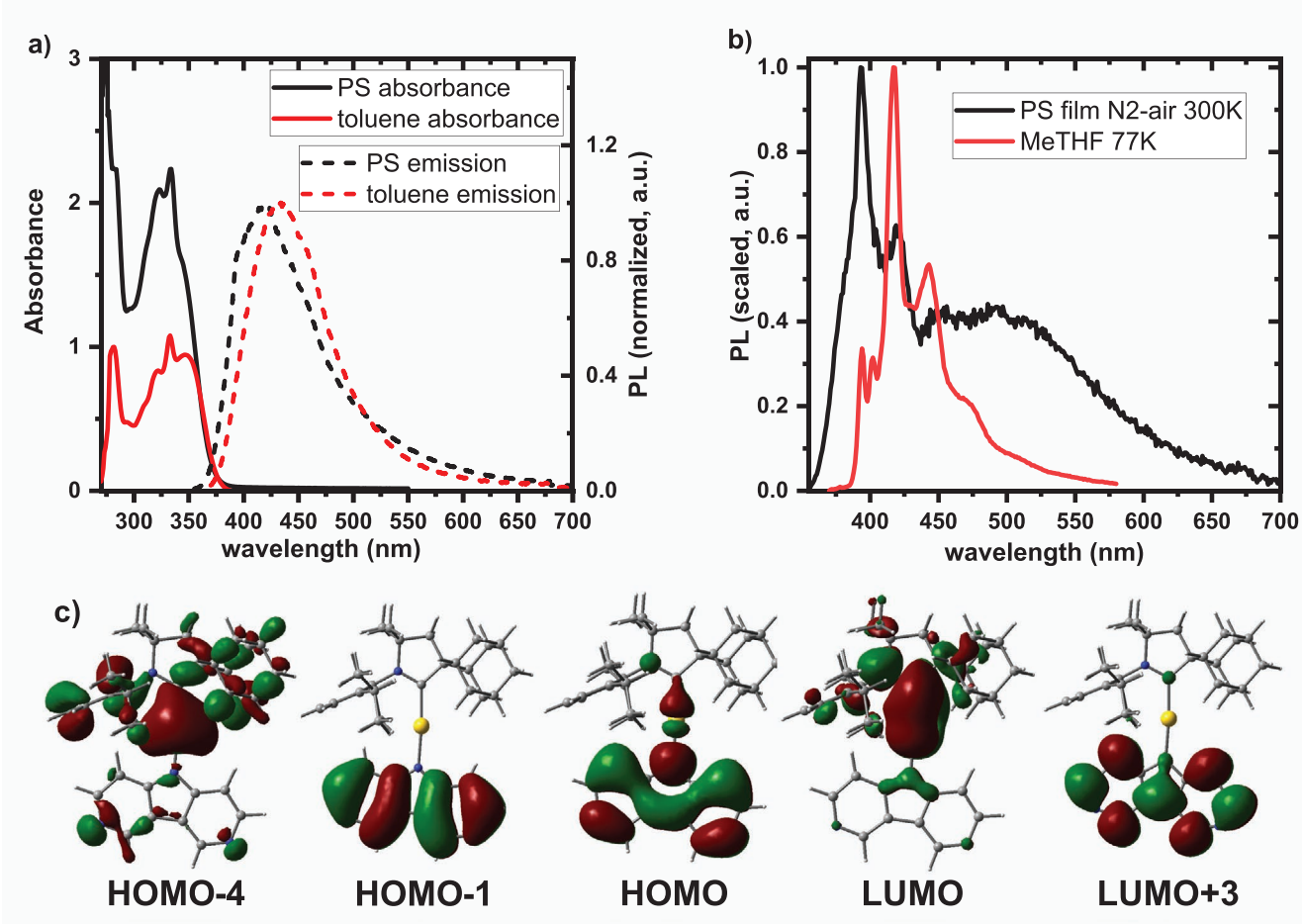

Figure 13. a) Steady-state emission and absorption spectra of 3 wt% PS host films and 0.5 mg mL^{-1} toluene solutions of 3,6-DiAza. b) Black line: weighted subtraction of emission spectra for 3,6-DiAza PS hosted films in air and under nitrogen. Red line: emission spectrum of 3,6-DiAza in MeTHF glass at 77 K. c) Main orbitals involved in the lowest excited states for 3,6-DiAza, calculated in S_0-optimized geometry.

(Figure 5). The 77 K MeTHF emission spectrum for 3,6-DiAza has an onset at 3.19 eV, which is 0.25 eV higher than unsubstituted CMA1 and 0.15 eV higher than Aza-3, the singly substituted variant with highest ^{3}LE energy (Table 1). Therefore, the extent of blueshift for both CT and ^{3}LE emission is greater than for any singly N-substituted variants. The increase in the ^{3}LE energy relative to CMA1 is more pronounced for the double aza-substitution complex 3,6-DiAza than for any singly N-substituted variants. However, unlike Aza-3, the relative increase in CT energy is greater than the increase in ^{3}LE energy for 3,6-DiAza, resulting in a positive CT–^{3}LE energy gap.

The excited state lifetime for 3,6-DiAza in toluene solution is 3.2 µs, slower than those of the singly-substituted variants except Aza-1 (Table 1). However, the PLQYs for 3,6-DiAza in solution and PS hosted film are 16% and 6%, respectively, which are the lowest values in the series of the aza-CMA materials. This indicates that the radiative decay rate in toluene is even slower than for Aza-1 (Table 1). As the CT–^{3}LE gap for 3,6-DiAza is estimated to be 70 meV, similar to Aza-4 and lower than Aza-1, this slow radiative decay rate represents a slight deviation from the trend followed by singly substituted variants as illustrated in Figure 10, though it remains broadly consistent.

3,6-DiAza shows a very deep-blue luminescence at 419 nm in PS hosted films, with some vibronic structure of the PL profile, which is more clearly visible in the difference spectrum (nitrogen-air PL). We attempted to extract the exact vibronic structure of the ^{3}LE phosphorescence at room temperature as shown on Figure S9, Supporting Information, however, time-resolved studies were precluded due to very long-lived luminescence of the 3,6-DiAza compound. The ^{3}LE emission is clearly visible in a frozen MeTHF solution at 77 K, with an excited state lifetime exceeding 11.8 ms.

TA spectroscopy of 3,6-DiAza in toluene and in PS films shows a rapid decay of the early-time species on a timescale of 3–4 ps (Figures S1,S2, Supporting Information for spectra and Figures S3,S5, Supporting Information for kinetics). This is the fastest rate in the aza-CMA series. The ESA of the early-time species demonstrates a broad profile with a peak around 650 nm, similar to CMA1 and the other aza-derivatives. In contrast, the late-time ESA for 3,6-DiAza shows little (if any) signal in the wavelength region probed for toluene solutions and only a weak ESA edge in PS hosted films, which is markedly different from what is seen in CMA1 and the other aza-derivatives. Due to this, triplet rise kinetics cannot be extracted for this material.

Theoretical calculations for 3,6-DiAza in S_0 geometry indicate that the lowest excited states (S_1 and T_1) are largely HOMO → LUMO and have a CT-like character (Table S6, Supporting Information; for relevant orbitals see Figure 13a). Calculations predict a CT blueshift of around 0.5 eV compared to CMA1 (Table 2), which is in good agreement with experimentally measured values in toluene solution. The HOMO → LUMO + 3 carbazole LE transition, which was the lowest ^{3}LE state for CMA1 and the singly substituted aza-derivatives, is no longer the lowest calculated ^{3}LE state for 3,6-DiAza (Table S8, Supporting Information). Instead, the states T_2 and T_3 are calculated to be predominantly of HOMO − 1 → LUMO + 3 and HOMO − 4 → LUMO in character, respectively, with the former localized mostly on the donor and the latter on the metal and the acceptor. The HOMO → LUMO + 3 triplet is calculated to be energetically above these states as T_4. These theoretical results suggest that the extent of blueshift for the CT and HOMO → LUMO + 3 for the ^{3}LE state in 3,6-DiAza becomes large enough that triplet states of different character may start to interfere in the photophysics of the deep-blue 3,6-DiAza material. The presence of these states cannot be explicitly confirmed from the experimental data collected, but the unusual structure observed in PL emission, the longer excited state lifetime in toluene and in a PS matrix, and the much different late-time ESA spectra compared to all other aza-derivatives indicate the involvement of such triplet states. We show a clear undesirable effect of the ^{3}LE proximity to the CT states which can be mitigated by simultaneously blueshifting both the lowest-lying CT and ^{3}LE states. This results in a sufficiently larger blueshift potentially allowing the involvement of the additional triplet states which have not been accessible before. This aspect needs to be considered in the further molecular design to develop the next generation of fast and deep-blue emitters.

4. Conclusions

Nitrogen substitution at various positions of the carbazole donor in gold-centered CMA materials allows the systematic variation of both the CT and ^{3}LE states. We find that a donor-centered ^{3}LE state lying near or below the CT states results in a mixed-type luminescence with contributions of TADF and/or phosphorescence with slow emission kinetics. For instance, in cases where the ^{3}LE state is significantly below the CT states, luminescence has a significant contribution from the long-lived ^{3}LE phosphorescence. When the ^{3}LE state is above the CT state, the emission lifetime shows only a weak dependence on the CT–^{3}LE gap, consistent with previous studies where emission in gold-centered CMAs is interpreted to occur predominantly via direct ^{3}CT–^{1}CT coupling. It is therefore generally desirable to have the donor ^{3}LE states well above the CT states to facilitate fast and deep-blue emission.

The electrochemistry supports the observed blueshift of CT (HOMO → LUMO) states in aza-substituted CMAs relative to unsubstituted CMA1 occurring due to lowering the HOMO energy level. We find that the extent of HOMO stabilization and subsequent CT luminescence blueshift varies with the location of the aza-substitution, being the greatest for Aza-1 and Aza-3. Theoretical calculations indicate that the LUMO + 3 orbital is involved in the ^{3}LE state (HOMO → LUMO + 3), with stabilization depending on the location of the aza-substitution position. The combined effects of HOMO and LUMO + 3 stabilization determine the energy shift of the ^{3}LE state. We show that simultaneous blueshift of CT and ^{3}LE states relative to CMA1 is only achieved in Aza-3, resulting in a blue CT emission with sub-microsecond excited state lifetimes and high quantum yields. Only the Aza-3 material is immune to the ^{3}LE phosphorescence in dilute PS-hosted films which is seen for all other aza-CMA materials. Analysis of the TA experiments indicates that the ISC rates are independent of the proximity between CT and LE states in all aza-CMA materials.

We demonstrate that the effect of aza-substitution on the HOMO and LUMO + 3 orbital energies, and therefore the CT and donor LE state energies, can be predicted (to a first

approximation) from relevant orbital coefficients at the substitution location. This results in a design principle allowing for simultaneous energy tuning of two excited states which are different in nature, via a simple synthetic modification of the CMA material. In the 3,6-DiAza complex, both the CT and ^{3}LE states are higher than for any of the singly substituted variants, which results in deep-blue luminescence but with several microsecond excited state lifetime and poor PLQY. This indicates the necessity to consider the impact of the chemical modification on the nonradiative rates and potential contribution of the higher-lying excited states when designing future generations of deep-blue and bright materials.

On the other hand, single aza-substitution in para-position to the pyrrole-nitrogen in the carbazole donor is a reliable molecular design strategy for blueshifting emissions while maintaining fast, bright PL characteristics and the CT character of the emission mechanism. This work demonstrates practical molecular design pathway toward the development of blue emitters for more stable deep-blue OLEDs based on CMA materials, where fast emission is a requirement to avoid material degradation and to improve the operational stability of blue OLED devices.

Supporting Information

Supporting Information is available from the Wiley Online Library or from the author.

Acknowledgements

This work was supported by the European Research Council, the Royal Society and the Academy of Finland. A.S.R. acknowledges support from the Royal Society (Grant nos. URF\R1\180288 and RGF\EA\181008) and Engineering and Physical Sciences Research Council (EPSRC grant EP/K039547/1). M.B. is an ERC Advanced Investigator Award holder (Grant no. 338944-GOCAT). M.L. acknowledges the Academy of Finland Flagship Programme, Photonics Research and Innovation (PREIN), decision 320166. (TD) DFT computations were made possible by use of the Finnish Grid and Cloud Infrastructure resources (urn:nbn:fi:research-infras-2016072533). A.-P.M.R. acknowledges support from the Royal Society (Grant no. RGF\EA\180041) and the Osk. Huttunen Foundation.

Conflict of Interest

The authors declare no conflict of interest.

Data Availability Statement

The data that support the findings of this study are available in the supplementary material of this article.

Keywords

carbazole, carbene-metal-amide, gold, phosphorescence, thermally activated delayed fluorescence

Received: February 9, 2022
Revised: April 5, 2022
Published online:

[1] D. Di, A. S. Romanov, L. Yang, J. M. Richter, J. P. H. Rivett, S. Jones, T. H. Thomas, M. A. Jalebi, R. H. Friend, M. Linnolahti, M. Bochmann, D. Credgington, *Science* **2017**, *356*, 159.
[2] A. S. Romanov, C. R. Becker, C. E. James, D. Di, D. Credgington, M. Linnolahti, M. Bochmann, *Chem. - Eur. J.* **2017**, *23*, 4625.
[3] A. S. Romanov, S. T. E. Jones, L. Yang, P. J. Conaghan, D. Di, M. Linnolahti, D. Credgington, M. Bochmann, *Adv. Opt. Mater.* **2018**, *6*, 1801347.
[4] P. J. Conaghan, C. S. B. Matthews, F. Chotard, S. T. E. Jones, N. C. Greenham, M. Bochmann, D. Credgington, A. S. Romanov, *Nat. Commun.* **2020**, *11*, 1758.
[5] F. Chotard, V. Sivchik, M. Linnolahti, M. Bochmann, A. S. Romanov, *Chem. Mater.* **2020**, *32*, 6114.
[6] H.-H. Cho, A. S. Romanov, M. Bochmann, N. C. Greenham, D. Credgington, *Adv. Opt. Mater.* **2021**, *9*, 2001965.
[7] R. Hamze, J. L. P. , D. Sylvinson, M. Jung, J. Cardenas, R. Haiges, M. Soleilhavoup, R. Jazzar, P. I. Djurovich, G. Bertrand, M. E. Thompson, *Science* **2019**, *363*, 601.
[8] T. Y. Li, D. S. Muthiah Ravinson, R. Haiges, P. I. Djurovich, M. E. Thompson, *J. Am. Chem. Soc.* **2020**, *142*, 6158.
[9] J. Eng, S. Thompson, G. Heather, D. Credgington, T. Penfold, *Phys. Chem. Chem. Phys.* **2020**, *22*, 4659.
[10] S. Thompson, J. Eng, T. Penfold, *J. Chem. Phys.* **2018**, *149*, 014304.
[11] J. Feng, A.-P. M. Reponen, A. S. Romanov, M. Linnolahti, M. Bochmann, N. Greenham, T. J. Penfold, D. Credgington, *Adv. Funct. Mater.* **2021**, *31*, 2005438.
[12] P. J. Conaghan, S. M. Menke, A. S. Romanov, A. J. Pearson, E. W. Evans, M. Bochmann, N. C. Greenham, D. Credgington, *Adv. Mater.* **2018**, *30*, 1802285.
[13] A. S. Romanov, L. Yang, S. T. E. Jones, D. Di, O. J. Morley, B. Drummond, A.-P. M. Reponen, M. Linnolahti, D. Credgington, M. Bochmann, *Chem. Mater.* **2019**, *31*, 3613.
[14] A. S. Romanov, S. T. E. Jones, Q. Gu, P. J. Conaghan, B. H. Drummond, J. Feng, F. Chotard, L. Buizza, M. Foley, M. Linnolahti, D. Credgington, M. Bochmann, *Chem. Sci.* **2020**, *11*, 435.
[15] a) M. Gernert, U. Müller, M. Haehnel, J. Pflaum, A. Steffen, *Chem. - Eur. J.* **2017**, *23*, 2206; b) M. Gernert, L. Balles-Wolf, F. Kerner, U. Müller, A. Schmiedel, M. Holzapfel, C. M. Marian, J. Pflaum, C. Lambert, A. Steffen, *J. Am. Chem. Soc.* **2020**, *142*, 8897; c) N. V. Tzouras, E. A. Martynova, X. Ma, T. Scattolin, B. Hupp, H. Busen, M. Saab, Z. Zhang, L. Falivene, G. Pisanó, K. Van Hecke, L. Cavallo, A. Steffen, C. S. J. Cazin, S. P. Nolan, *Chem. - Eur. J.* **2021**, *27*, 11904.
[16] R. Hamze, S. Shi, S. C. Kapper, D. Sylvinson, M. R. L. Estergreen, M.-C. Jung, A. C. Tadle, R. Haiges, P. I. Djurovich, J. L. Peltier, R. Jazzar, G. Bertrand, S. E. Bradforth, M. E. Thompson, *J. Am. Chem. Soc.* **2019**, *141*, 8616.
[17] A. S. Romanov, F. Chotard, J. Rashid, M. Bochmann, *Dalton Trans.* **2019**, *48*, 15445.
[18] A. S. Romanov, M. Linnolahti, M. Bochmann, *Dalton Trans.* **2021**, *50*, 17156.
[19] A. Endo, K. Sato, K. Yoshimura, T. Kai, A. Kawada, H. Miyazaki, C. Adachi, *Appl. Phys. Lett.* **2011**, *98*, 083302.
[20] H. Uoyama, K. Goushi, K. Shizu, H. Nomura, C. Adachi, *Nature* **2012**, *492*, 234.
[21] I. R. Gould, J. A. Boiani, E. B. Gaillard, J. L. Goodman, S. Farid, *J. Phys. Chem. A* **2003**, *107*, 3515.
[22] B. T. Lim, S. Okajima, A. K. Chandra, E. C. Lim, *Chem. Phys. Lett.* **1981**, *79*, 22.
[23] J. Gibson, A. P. Monkman, T. J. Penfold, *ChemPhysChem* **2016**, *17*, 2956.
[24] X. K. Chen, S. F. Zhang, J. X. Fan, A. M. Ren, *J. Phys. Chem. C* **2015**, *119*, 9728.
[25] C. M. Marian, *J. Phys. Chem. C* **2016**, *120*, 3715.

[26] M. K. Etherington, J. Gibson, H. F. Higginbotham, T. J. Penfold, A. P. Monkman, *Nat. Commun.* **2016**, *7*, 13680.
[27] J. Feng, L. Yang, A. S. Romanov, J. Ratanapreechachai, S. T. E. Jones, A.-P. M. Reponen, M. Linnolahti, T. J. H. Hele, A. Köhler, H. Bässler, M. Bochmann, D. Credgington, *Adv. Funct. Mater.* **2020**, *30*, 1908715.
[28] N. C. Giebink, B. W. D'Andrade, M. S. Weaver, P. B. Mackenzie, J. J. Brown, M. E. Thompson, S. R. Forrest, *J. Appl. Phys.* **2008**, *103*, 044509.
[29] S. Scholz, D. Kondakov, B. Lüssem, K. Leo, *Chem. Rev.* **2015**, *115*, 8449.
[30] R. A. Abramovitch, I. D. Spenser, *Adv. Heterocycl. Chem.* **1964**, *3*, 79.
[31] Y. Im, J. Y. Lee, *Chem. Commun.* **2013**, *49*, 5948.
[32] C. S. Oh, C. W. Lee, J. Y. Lee, *Chem. Commun.* **2013**, *49*, 10181.
[33] G. H. Kim, R. Lampande, J. B. Im, J. M. Lee, J. Y. Lee, J. H. Kwon, *Mater. Horiz.* **2017**, *4*, 619.
[34] C. R. Hall, A. S. Romanov, M. Bochmann, S. R. Meech, *J. Phys. Chem. Lett.* **2018**, *9*, 5873.
[35] J. Feng, E. J. Taffet, A.-P. M. Reponen, A. S. Romanov, Y. Olivier, V. Lemaur, L. Yang, M. Linnolahti, M. Bochmann, D. Beljonne, D. Credgington, *Chem. Mater.* **2020**, *32*, 4743.
[36] O. B. Smirnova, T. V. Golovko, V. G. Granik, *Pharm. Chem. J.* **2011**, *45*, 389.
[37] A. Abdurahman, T. J. H. Hele, Q. Gu, J. Zhang, Q. Peng, M. Zhang, R. H. Friend, F. Li, E. W. Evans, *Nat. Mater.* **2020**, *19*, 1224.
[38] J. Föller, C. M. Marian, *J. Phys. Chem. Lett.* **2017**, *8*, 5643.
[39] D. Tanaka, T. Takeda, T. Chiba, S. Watanabe, J. Kido, *Chem. Lett.* **2007**, *36*, 262.
[40] S. J. Su, Y. Takahashi, T. Chiba, T. Takeda, J. Kido, *Adv. Funct. Mater.* **2009**, *19*, 1260.
[41] P. L. Dos Santos, F. B. Dias, A. P. Monkman, *J. Phys. Chem. C* **2016**, *120*, 18259.